Computational Study of Model Pd−Zn Nanoclusters and Their Adsorption Complexes with CO Molecules

Konstantin M. Neyman,*,† Riadh Sahnoun, Chan Inntam, Sunantha Hengrasmee,‡ and Notker Rösch*

Department Chemie, Technische Universität München, 85747 Garching, Germany

Received: January 13, 2004; In Final Form: February 24, 2004

Using an all-electron scalar relativistic density functional method, we studied bimetallic cuboctahedral nanoscale clusters $Pd_{140-n}Zn_n$ ($n = 0$, 8, 24, 32) as local models of the active component of novel Pd/ZnO catalysts for methanol steam reforming. As recently demonstrated (Yudanov, I. V, et al. *J. Chem. Phys*. **2002**, *117*, 9887; Yudanov, I. V., et al. *J. Phys. Chem. B* **2003**, *107*, 255), such compact model clusters provide a quantitatively accurate description of adsorption properties of single-crystal metal surfaces as well as supported metal particles. The calculated average cluster cohesive energy decreases gradually when the number of Zn atoms increases: each of them introduces a destabilization by ~1 eV. Zn atoms preferentially occupy positions in the surface layer of the clusters. A small transfer of electron density from Zn to Pd atoms was found. To probe how adsorption properties of bimetallic species change relative to those of the reference cluster Pd_{140}, we studied complexes with CO molecules adsorbed on 3-fold hollow Pd_3 sites of (111) cluster facets. CO adsorption energies were calculated notably smaller when Zn atoms are located in the subsurface layer of the clusters; on the other hand, Zn atoms in the surface layer affected the CO adsorption energy only slightly. Calculated CO adsorption energies and vibrational C−O frequencies do not correlate, reflecting the different origin of these properties.

Introduction

Steam reforming of methanol over metal catalysts is one of the most attractive processes for producing in-situ H_2 as an energy carrier alternative to conventional fuels.[1] Novel efficient catalysts based on a Pd/ZnO system have been proposed for the steam reforming reaction.[2,3] The high performance of these catalysts was attributed to Pd−Zn alloy particles.[4,5] Despite the importance of Pd−Zn moieties, only very limited electronic and structural information on them at the atomic level has been available until very recently,[6,7] thus preventing a detailed characterization of the active component of the catalyst and understanding its function.

This lack of structural and electronic information about the surface of bimetallic Pd−Zn species prompted us to initiate systematic density functional (DF) slab model calculations of these materials that address diverse aspects important for elucidating their stability, structure, and reactivity.[8−10] A comparative study of surface energies of binary (1:1) PdZn alloys with CuAu-$L1_0$ structure revealed that (111) and (100) surfaces exposing stoichiometric layers are more stable than (001) and (110) surfaces which consist of alternating Pd and Zn layers; therefore, surfaces with the (111) and (100) orientations probably form preferentially under ambient experimental conditions.[8] We also explored surface segregation of Zn and Pd in supported PdZn alloy films of the above structure and found that it depends significantly on the support; at stoichiometric surfaces of 1:1 alloy, segregation of neither Zn nor Pd was calculated favorable whereas in films rich in Zn or Pd segregation of the dominant component was found possible.[9] Our most recent computational slab model study was devoted to the structure and energetics of adsorption complexes relevant for methanol decomposition on the single-crystal PdZn(111) surface.[10]

The electronic structure investigations just outlined focused on idealized situations modeling rather extended (111) terraces of PdZn alloy catalysts with a low concentration of various defects. More realistically, active sites of supported metal catalytic materials can be represented by so-called model catalysts[11,12] which consist of well-ordered nanoscale metal particles deposited on oxide films. Such model catalysts are less complex than "real" catalysts although they feature, at variance with regular single-crystal metal surfaces, most of the irregularities inherent to real catalysts, such as edge and step sites as well as regular sites in their proximity. Recently, we proposed an efficient computational strategy for modeling extended terraces[13] as well as supported metal nanoparticles;[14] that strategy relies on symmetric three-dimensional model clusters which are terminated by low-index surfaces and contain 100 or more metal atoms. With this strategy, we were able to unravel bonding and vibrations of CO molecules adsorbed at Pd nanoclusters[13,14] and we clarified the location of light atom elements in the subsurface region of Pd nanoparticles.[15]

In this work, we consider a series of model octahedral Pd−Zn nanoscale clusters $Pd_{140-n}Zn_n$ ($n = 0$, 8, 24, 32) and their complexes with CO molecules adsorbed on 3-fold hollow sites built by three Pd atoms in the center of (111) facets. To the best of our knowledge, this is the first high-level electronic structure study of *bimetallic* clusters containing over 100 heavy-

* Corresponding authors. E-mail addresses: roesch@ch.tum.de, konstantin.neyman@ub.edu.

† Present address: ICREA (Institució Catalana de Recerca i Estudis Avançats) and Departament de Química Física, Universitat de Barcelona, C/ Marti i Franques 1, 08028 Barcelona, Spain.

‡ Permanent address: Department of Chemistry, Khon Kaen University, Thailand.

10.1021/jp049830f CCC: $27.50
Published on Web 04/02/2004

element atoms and approaching the size of 2 nm. Thus, this paper extends the application area of our novel computational strategy to investigate surface properties of transition metal single-crystal and polycrystalline materials by employing three-dimensional cluster models. A special goal of the present work is to shed a light on the influence of Zn admixtures to Pd nanoclusters at varying (relatively low) concentrations (*i*) on the electronic structure, the segregation of the Zn component, and the stability of model Pd−Zn nanoparticles, as well as (*ii*) on their adsorption properties monitored by the binding energy and C−O vibrational frequency of adsorbed carbonyl molecules.

Computational Details and Models

We performed all-electron calculations using the linear combination of Gaussian-type orbitals fitting-functions density functional (LCGTO-FF-DF) method[16] as implemented in the parallel code ParaGauss.[17,18] We used a scalar relativistic variant of the LCGTO-FF-DF method[19−21] which employs a second-order Douglas-Kroll transformation to decouple electronic and positronic degrees of freedom of the Dirac-Kohn−Sham equation. We solved the Kohn−Sham equation self-consistently in the local density approximation (LDA; VWN parametrization[22]); subsequently, we calculated the total energy in a generalized-gradient approximation (GGA) using the self-consistent LDA electron density and the BP exchange-correlation functional.[23,24] This computational strategy is very economic, yet sufficiently accurate for geometric parameters, binding energies, and vibrational frequencies;[25] our benchmark self-consistent BP calculations of CO adsorption energies on Pd nanoclusters corroborated its high accuracy (within 1%).[15] Where explicitly specified in the following, we also employed a modern GGA functional (PBEN[26]) for comparison with the BP results.

The computational parameters were chosen to be consistent with those of our previous studies.[13−15] For Pd atoms, we used an orbital basis set[27] extended to (18*s*,13*p*,9*d*) by adding one *s* exponent (0.0135), two *p* exponents (0.0904, 0.2143), and one *d* exponent (0.097); it was contracted in a generalized fashion to [7*s*,6*p*,4*d*] using relativistic VWN atomic eigenvectors. To evaluate the classical Coulomb contribution to the electron−electron interaction, the electron density was represented with the help of an auxiliary basis set;[16] for Pd it was of the size (17*s*,6r^2,5*p*,5*d*). For Zn atoms we employed a (14*s*,9*p*,5*d*) orbital basis set,[27] extended by one *s* exponent (0.39748), two *p* exponents (0.11610, 0.30312), and a *d* exponent (0.16366), and contracted to [6*s*,5*p*,3*d*]; the auxiliary charge density basis set was (15s,11r^2,5*p*,5*d*). C and O atoms were described by orbital basis sets of the type (14*s*,9*p*,4*d*)[28] using the original general contraction [6*s*,5*p*,2*d*] and by auxiliary basis sets of the type (14*s*,9r^2,5*p*,5*d*). For every atom, the auxiliary basis was constructed as follows: the exponents of *s* and r^2 fitting functions were generated by scaling (all or selected) *s* and *p* orbital exponents, respectively, using a standard procedure;[16] "polarization exponents" were chosen as geometric series with factor 2.5, starting with 0.1 for *p* and 0.2 for *d* exponents.

Our benchmark calculations did not reveal open-shell configurations for the clusters $Pd_{140-n}Zn_n$. For monometallic palladium clusters, which have a potentially larger propensity to exhibit unpaired spins than PdZn clusters, spin averaging introduces marginal errors.[29] For instance, already for Pd_{85}, this was found to hold for such a sensitive property as the cohesive energy. Furthermore, recall that spin polarization effects decrease with growing cluster size. Therefore, in the following we will discuss only results obtained in a spin-restricted fashion. Throughout, we applied the technique of fractional occupation numbers[16] (with a Gaussian level broadening of 0.1 eV) to ensure convergence of the SCF process. When probing adsorption properties, we kept the geometric parameters of all bare model clusters $Pd_{140-n}Zn_n$ fixed (see below); we optimized only the positions of adsorbed CO molecules, oriented according to the symmetry group O_h. For that, we consecutively varied Pd−C and C−O distances until changes were below 0.5 pm, using BP energies. We corrected the CO adsorption energy for the basis set superposition error via the counterpoise technique (0.22−0.25 eV);[30] one-quarter of these corrections were due to the incompleteness of the CO basis set. We approximated the harmonic C−O stretching vibration by the C−O internal mode, keeping the CO center of mass fixed; for this purpose, we fitted a polynomial of degree 4 to five total energy values near the minimum of the potential curve.

Designing realistic models of Pd−Zn catalysts is inherently a complicated problem. In fact, even focusing solely on the active bimetallic particles without a support,[31,32] one needs to address simultaneously many aspects of the species to be represented. Among them are (*i*) the size range, (*ii*) the overall stoichiometry as well as the mutual positions of the constituting Pd and Zn atoms, (*iii*) the types of the facets exposed and their roughness, and finally (*iv*) the adsorption sites to be probed. Also, the computational effort required to treat such complex models has to remain within reasonable limits, ensuring the feasibility of the calculations.

Here, we focused on Pd−Zn moieties that are sufficiently large to be approximated by clusters with metal−metal (M−M) distances corresponding to bulk samples.[13] We selected a range of relatively low Zn concentrations, up to ∼25%, in the Pd−Zn moieties. Thus, the overall structural arrangement and all M−M distances, 275 pm, of our bimetallic cluster models were chosen as measured for bulk palladium.[33] This is quite different from the CuAu ($L1_0$-type) structure with space group *P*4/*mmm*, that is featured by PdZn alloys with a Pd/Zn atomic ratio close to 1,[34] that appear to exhibit the highest catalytic performance in steam reforming of methanol.[4,5] For the latter bulk structure, our periodic calculations with the PW91 exchange-correlation potential[35] furnished optimized distances *r*(Pd−Pd) = 293 pm and *r*(Pd−Zn)=268 pm.[8] These values deviate notably and in different directions (by 18 pm and −7 pm, respectively) from the M−M bond lengths that we employed in the nanocluster models which we chose to have a significantly lower Zn content. As mentioned above, M−M distances were kept frozen in the present model study to separate the more pronounced electronic effects and those caused by a variation of the mutual positions of Pd and Zn atoms from the modest effect of changes of M−M bond lengths.[13−15] (Note that the average nearest-neighbor Pd−Pd distance in the cluster model Pd_{140} optimized at the LDA-VWN level is 268.3 pm.[13]) The mutual positions of Pd and Zn atoms comply with O_h symmetry which we imposed on all cluster models.

According to our slab model calculations,[8] hexagonal (111) surfaces of PdZn alloys are characterized by the lowest surface energy. Therefore, our cluster models were designed to expose preferentially (111) facets: the cuboctahedral cluster models M_{140} (Figure 1a) were obtained by truncating the corresponding octahedral clusters M_{146} to yield eight hexagonal (111) facets. Adsorption sites on these flat facets are rather close to edges. From experimental investigations[36,37] as well as from periodic slab model calculations[38,39] it is known that 3-fold hollow sites on the Pd(111) surface are energetically favored for CO adsorption at low coverage; therefore, keeping in mind the low concentration of Zn in the bimetallic moieties under investiga-

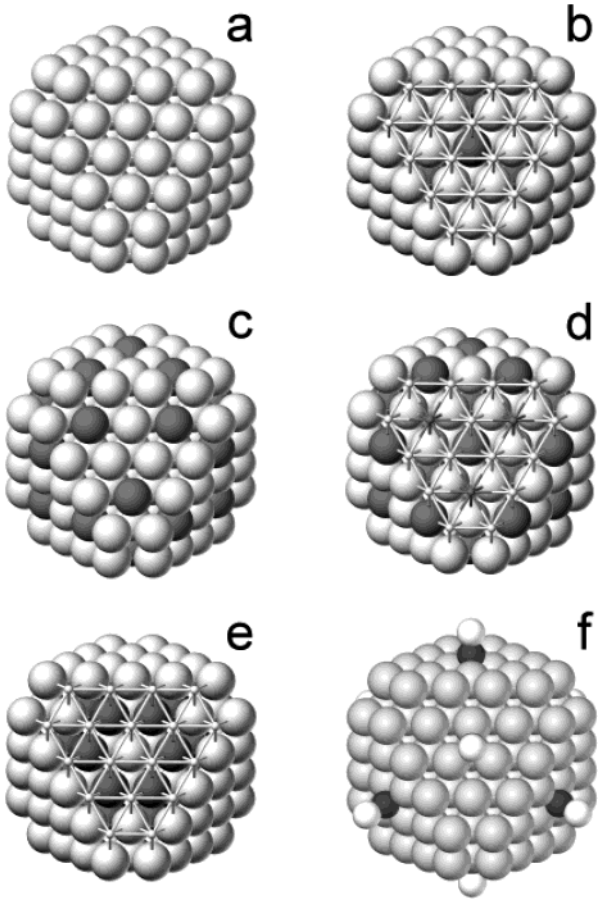

Figure 1. Sketches of the cuboctahedral model nanoclusters: (a) Pd_{140}, (b) $Pd_{132}Zn_8(0,8)$, (c) $Pd_{116}Zn_{24}(24,0)$, (d) $Pd_{108}Zn_{32}(24,8)$, (e) $Pd_{116}Zn_{24}(0,24)$, (f) a representative adsorption complex $Pd_{140}(CO)_8$. The numbers of Zn atoms in the surface and subsurface layers, respectively, are given in parentheses. In panels b, d, and e, the first layer of one (111) facet is depicted as a network of bonds only to allow a better description of the subsurface region.

tion, we probed this site by adsorbed CO molecules. For that purpose, we kept intact the central upper-layer Pd_3 moiety on each of the eight (111) facets in all our models, but we partially substituted Zn atoms for nearby Pd atoms. The resulting series of substrate clusters comprises, beyond the reference Pd_{140} (Figure 1a), the following four bimetallic systems: $Pd_{132}Zn_8(0,8)$, $Pd_{116}Zn_{24}(24,0)$, $Pd_{108}Zn_{32}(24,8)$, $Pd_{116}Zn_{24}(0,24)$; here, the numbers in parentheses refer to Zn atoms in the surface and subsurface layers, respectively (Figure 1b−e). In $Pd_{132}Zn_8(0,8)$, eight Zn atoms are located in the second layer of the cluster, just beneath the central Pd_3 triangle of each (111) facet whereas 24 Zn atoms of $Pd_{116}Zn_{24}(24,0)$ are in nearest-neighboring first-layer positions of the Pd_3 moiety. The model $Pd_{108}Zn_{32}(24,8)$ combines Zn positions of the former two systems. Finally, the 24 Zn atoms of the cluster $Pd_{116}Zn_{24}(0,24)$ are arranged as a cage of eight Zn_6 rings with short Zn−Zn contacts of 275 pm. These Zn atoms substitute six subsurface Pd atoms of every (111) facet that surround the position occupied by Zn in $Pd_{132}Zn_8(0,8)$ particle; each of the six positions is shared by two second-layers of the adjacent (111) facets. We monitored alterations of electronic properties and the reactivity of these bimetallic clusters as reflected by bonding and vibrations of single CO adsorbates positioned on the central *hcp* (hexagonal close packed) sites of their (111) facets (Figure 1f).

Previously, we demonstrated[13] that three-dimensional cluster models containing as many as 140 metal atoms furnish *all* calculated adsorption parameters for CO molecules essentially converged with respect to the cluster size; this includes the adsorption energy as the most delicate observable.[40,41] Our symmetric cluster models contain a considerably larger fraction of metal atoms with high coordination numbers compared to "planar" ("two-dimensional") cluster models that have been commonly used in chemisorption studies.[40,41] The boundary metal atoms of such conventional models are a source of inaccuracy and possible cluster artifacts; at variance, boundary atoms of three-dimensional cluster models as employed here are represented in a much more realistic fashion.

Results and Discussion

We will first discuss calculated observables for bare bimetallic clusters $Pd_{140-n}Zn_n$ and the reference system Pd_{140}, and present a comparative analysis of these data. Then, we will address the CO adsorption properties of these clusters.

Properties of Bare Pd−Zn Clusters. The mixed-metal substrate clusters $Pd_{140-n}Zn_n$ (Figure 1b−e) contain different numbers of Zn atoms that substitute Pd atoms of the reference cluster Pd_{140} (Figure 1a) in the surface layer or just beneath the surface layer or both. This "alloying" results in varying numbers of homo- and heteroatomic nearest-neighbor M−M contacts ("bonds"). The species $Pd_{132}Zn_8(0,8)$, $Pd_{116}Zn_{24}(24,0)$, and $Pd_{108}Zn_{32}(24,8)$ feature 96, 216, and 312 Pd−Zn bonds, respectively, which are formed at the expense of Pd−Pd bonds of the Pd_{140} reference. None of these clusters exhibits direct Zn−Zn contacts; however, such contacts are present in the cluster $Pd_{116}Zn_{24}(0,24)$ which features 288 new types of nearest-neighbor M−M contacts compared to Pd_{140}, 216 of type Pd−Zn, and 72 of type Zn−Zn. The Zn−Zn bonds comprise a new feature which is expected to be manifested in qualitatively different properties of the particle $Pd_{116}Zn_{24}(0,24)$ compared to its $Pd_{140-n}Zn_n$ analogues.

The species $Pd_{116}Zn_{24}(0,24)$ and $Pd_{116}Zn_{24}(24,0)$ with the same number of Zn atoms but located in the subsurface layer and on the surface, respectively, can be considered as models for addressing the phenomenon of segregation, namely, enrichment of one of the alloy components in the surface by exchange with subsurface atoms. Recently, we studied segregation at the surface of Pd−Zn alloys in detail by means of slab model calculations and we found this process to be very sensitive to the local and overall structure as well as to the stoichiometry of the material.[9] According to the present cluster model results, the total energy of the system $Pd_{116}Zn_{24}(24,0)$ with all Zn atoms on the surface is 0.20 eV per Zn atom lower than that of the system $Pd_{116}Zn_{24}(0,24)$ with all Zn atoms located in subsurface positions. Surface positions of Zn atoms are favored as a consequence of the fact that 72 new Pd−Pd bonds are formed from 72 weaker Zn−Zn bonds while the number of Pd−Zn bonds remains the same in both clusters. This finding agrees with the slab model result that in films rich in Zn [such as the subsurface layer of $Pd_{116}Zn_{24}(0,24)$], segregation of Zn can be favored.[9] The notable cohesive energy gain of 0.20 eV per surface Zn atom can be translated into a cluster stabilization of 0.07 eV per Zn−Zn bond exchanged for a Pd−Pd bond. From these values, the average cohesive energy per atom, $E_b/140 = 3.07$ eV, of the cluster Pd_{140} (Table 1), and the average coordination number $N_{av} = 9.09$ of Pd atoms of that cluster,[13] one can approximately associate each Pd−Pd contact with an energy gain of 0.34 eV and consequently each Zn−Zn contact (disfavored by 0.07 eV) with an energy gain of 0.27 eV. Note that the latter estimates differ notably from the bond energies of the dimer molecules Pd_2 and Zn_2, namely, 1.0−1.4 eV[42,43]

TABLE 1: Calculated Energies[a] (in eV) for Model Nanoclusters $Pd_{140-n}Zn_n$ (n = 0, 8, 24, 32)

	Pd_{140}	$Pd_{132}Zn_8$(0,8)	$Pd_{116}Zn_{24}$(24,0)	$Pd_{108}Zn_{32}$(24,8)	$Pd_{116}Zn_{24}$(0,24)
$E_b/140$	3.07	3.01	2.89	2.83	2.85
$\Delta E_b/n$		−1.04	−1.04	−1.05	−1.24
ϵ_F	−5.13	−5.20	−4.94	−5.00	−5.17
$\Delta\epsilon_{Pd4d}$	−2.05	−1.99	−1.99	−1.92	−1.89
$\Delta\epsilon_{Pd4d}(Pd_3)$	−2.07	−2.04	−1.99	−2.01	−2.04

[a] $E_b/140 = [n \times E(Zn) + (140 - n) \times E(Pd) - E(Pd_{140-n}Zn_n)]/140$ is the average binding (cohesive) energy of $Pd_{140-n}Zn_n$ per atom, where $E(X)$ is the total energy of the species X; $\Delta E_b/n = \{[n \times E(Zn) + (140 - n - E(Pd_{140-n}Zn_n)]/n$ is the average contribution of each of the n Zn atoms to the change of the overall cohesive energy $E_b(Pd_{140-n}Zn_n)$ with respect to $E_b(Pd_{140})$; $\Delta\epsilon_{Pd4d}$ and $\Delta\epsilon_{Pd4d}(Pd_3)$ are the centers of the Pd 4*d* density of states with respect to the cluster Fermi energy ϵ_F, total and local (for the Pd_3 moiety in the center of (111) facets), respectively.

and 0.03 eV,[43] respectively. These strong differences were not unexpected; they reflect the rather different nature of M−M interactions in bulk metals and molecular species.

For the four model clusters which do not exhibit nearest-neighbor Zn−Zn moieties, the calculated average binding (cohesive) energy per atom, $E_b/140$, decreases when the number of Zn atoms increases (Table 1): Pd_{140} − 3.07 eV, $Pd_{132}Zn_8$(0,8) − 3.01 eV, $Pd_{116}Zn_{24}$(24,0) − 2.89 eV, $Pd_{108}Zn_{32}$(24,8) − 2.83 eV. If one translates this reduced overall stability of the model bimetallic clusters upon substitution of Zn for Pd atoms into an alteration of the cluster cohesive energy per Zn atom, one finds a rather large and, interestingly, essentially constant value of about 1.05 eV, for the three bimetallic systems just mentioned which do not show nearest-neighbor Zn−Zn contacts. As discussed above, the cluster $Pd_{116}Zn_{24}$(0,24) with its weaker Zn−Zn "bonds" features a more pronounced destabilization per Zn atom, 1.24 eV. On the basis of these results, one concludes that in Pd−Zn alloy particles *exhibiting fcc structure*, homoatomic Pd−Pd bonding interactions are somewhat stronger than heteroatomic Pd−Zn ones.

This seems to be at variance with our slab model data[9] calculated for the CuAu ($L1_0$-type) structure of Pd−Zn alloys, which correspond to considerably larger Zn concentrations;[34] the slab model results were rationalized in terms of the Pd−Zn bond strength prevailing over Pd−Pd interactions.[9] However, the alteration of the Pd−Pd and Pd−Zn bond energies in alloy moieties is caused by significantly different Pd−Pd bond lengths in the *fcc* structure of the nanoparticles and in the CuAu ($L1_0$-type) structure of slabs. Indeed, the optimized slab model distance r(Pd−Pd) = 293 pm[9] reveals considerable elongation of Pd−Pd contacts and thus, a notable *destabilization* of Pd−Pd interactions compared to those in the present cluster models, where Pd atoms are at the equilibrium Pd−Pd distance of Pd bulk, 275 pm. On the other hand, Pd−Zn interatomic spacings in the slab models (268 pm) and the cluster models (275 pm) both appear to be close to the "optimum energy" value r(Pd−Zn) ≅ 271 pm, estimated as the sum of Pd and Zn atomic radii in metals, 137.6 pm (Pd) and 133.5 pm (Zn);[44] therefore, destabilization of the Pd−Zn interaction, unlike the Pd−Pd one, is expected to be small in both the *fcc* and CuAu ($L1_0$-type) structures. These considerations indicate that the preference of the Pd−Pd and Pd−Zn bond strengths is a very delicate property that can be affected by a mere modification of the structural arrangement of Pd−Zn alloy species due to a phase transition. Consequences of this interesting feature are important for accounting structural transformations of materials based on Pd−Zn alloys.

One of the crucial parameters characterizing the electronic structure is the cluster Fermi energy, ϵ_F.[16] The Fermi energies of $Pd_{140-n}Zn_n$ clusters spread over a narrow interval, from −5.20 to −4.94 eV (Table 1); they correlate with neither the amount nor the location of Zn atoms. The former finding is consistent with the low values of Zn admixtures. The presence of Zn atoms in the clusters slightly destabilizes the center of the Pd 4*d* band; see the energy differences $\Delta\epsilon_{Pd4d}$ with respect to ϵ_F which indicate upward shifts by 0.06−0.16 eV (Table 1). Not unexpectedly, the relative positions $\Delta\epsilon_{Pd4d}(Pd_3)$ of the 4*d* manifold of the three Pd atoms, which are situated in the middle of the eight hexagonal facets and form the 3-fold hollow adsorption site for CO probes (see next subsection), show even smaller relative upward shifts, 0.03−0.08 eV, compared to the parent cluster Pd_{140}.

Of particular interest is the charge redistribution between Pd and Zn atoms in the bimetallic clusters. However, one should keep in mind that *all* widely used approaches to assign electron density to certain atomic centers are inherently approximate, equivocal, and depend on the definition: there is no quantum mechanical observable that represents atomic charges in multinuclear moieties. In the present study, for the *qualitative* purposes, we used Mulliken charges as well as the somewhat better grounded potential-derived charges (PDCs)[45] that reproduce the electrostatic field outside the clusters.

Based merely on atomic electronegativity values (Pd 1.4, Zn 1.7),[44] Zn atoms might be expected to acquire electron density, despite their stable electron configuration $d^{10}s^2$. However, in line with this saturated configuration, biased against electron gain, Mulliken charges on Zn atoms are positive: 0.60 e − $Pd_{132}Zn_8$(0,8), 0.49 e − $Pd_{116}Zn_{24}$(0,24), 0.45 e − $Pd_{116}Zn_{24}$(24,0), 0.45 e for Zn(24,0) atoms, and 0.64 e for Zn(0,8) atoms of $Pd_{108}Zn_{32}$(24,8), with the corresponding electron populations $3d^{9.92}4s^{1.01}4p^{0.47}$, $3d^{9.97}4s^{0.96}4p^{0.58}$, $3d^{9.96}4s^{1.10}4p^{0.49}$, $3d^{9.95}4s^{1.10}4p^{0.50}$, $3d^{9.92}4s^{1.03}4p^{0.41}$, respectively. Thus, these Mulliken charges suggest electron-depleted Zn centers and this situation is corroborated by PDC values. The latter characteristics for Zn atoms are positive albeit notably smaller: 0.14 e for $Pd_{132}Zn_8$(0,8), 0.10 e for $Pd_{116}Zn_{24}$(0,24), 0.25 e for $Pd_{116}Zn_{24}$(24,0), 0.25 e for Zn(24,0) atoms, and 0.18 e for Zn(0,8) atoms of $Pd_{108}Zn_{32}$(24,8). To estimate more correctly the charge redistribution due to the introduction of Zn atoms, these PDC values should be calibrated against the charges on Pd atoms of the reference cluster Pd_{140} in the positions where Zn atoms are located. Already Pd atoms in these "Zn" positions are somewhat electronically depleted [0.10 e in Zn(0,8), 0.04 e in Zn(0,24), and 0.09 e in Zn(24,0)]; therefore, such a calibration results in a rather modest specific electron density transfer from Zn atoms in $Pd_{140-n}Zn_n$ cluster models, 0.04−0.16 e. Both Mulliken and potential-derived charges of Zn atoms are essentially defined by the position in the cluster and only slightly affected by the presence or the absence of other Zn atoms in the species.

Finally, one can try to characterize the charge state of the three Pd atoms in the center of hexagonal facets of all the moieties $Pd_{140-n}Zn_n$ which are to form the μ_3 adsorption sites. The Mulliken charges of these symmetry-equivalent Pd atoms are negative (Mulliken populations in parentheses): −0.32 e ($4d^{8.69}5s^{1.36}5p^{0.27}$) − Pd_{140}, −0.29 e ($4d^{8.74}5s^{1.28}5p^{0.27}$) − $Pd_{132}Zn_8$(0,8), −0.33 e ($4d^{8.79}5s^{1.25}5p^{0.29}$) − $Pd_{116}Zn_{24}$(0,24), −0.45

TABLE 2: Calculated Characteristics[a] of Adsorption Complexes of Model Nanoclusters $Pd_{140-n}Zn_n$ with Eight CO Molecules on the Central *hcp* Pd_3 Sites of the (111) Facets

observable	Pd_{140}[b]	$Pd_{132}Zn_8$(0,8)	$Pd_{116}Zn_{24}$(24,0)	$Pd_{108}Zn_{32}$(24,8)	$Pd_{116}Zn_{24}$(0,24)
r(Pd−C), pm	206.3	207.3	207.4	206.3	203.1
r(C−O), pm	118.9	118.6	118.9	118.9	118.9
D_e, eV	1.75	1.61	1.75	1.63	1.25
D_e,[c] eV	1.47	1.32	1.47	1.36	0.94
ω(C−O), cm^{-1}	1748	1758	1751	1745	1755
ϵ_F, eV	−5.31	−5.38	−5.14	−5.19	−5.30
$\Delta\epsilon_{Pd4d}$, eV	−2.09	−2.02	−2.05	−1.98	−2.01
$\Delta\epsilon_{Pd4d}(Pd_3)$, eV	−2.44	−2.42	−2.39	−2.44	−2.67

[a] BP level: r(Pd−C), r(C−O) represent interatomic distances, D_e is the adsorption energy per CO molecule corrected for the basis set superposition error, ω(C−O) is the harmonic frequency of the C−O vibration; other notations as defined in Table 1. [b] Ref 13. [c] This is the PBEN adsorption energy calculated for the geometry optimized at the BP level (PBEN//BP).

e ($4d^{8.84}5s^{1.27}5p^{0.34}$) − $Pd_{116}Zn_{24}$(24,0), −0.42 e ($4d^{8.88}5s^{1.21}5p^{0.33}$) − $Pd_{108}Zn_{32}$(24,8). Again, PDC values support this direction of charge redistribution, although they feature significantly reduced "charging" of the Pd_3 atoms; it ranges from only −0.2 e in $Pd_{132}Zn_8$ to −0.07 e in $Pd_{116}Zn_{24}$(24,0).

Adsorption Properties of Pd−Zn Clusters. The adsorption properties of mixed-metal Pd−Zn nanoparticles and, in particular, their reactivity can be understood in terms of their electronic structure parameters. A very simplified argument invokes mixing of d^{10} (Pd) and $d^{10}s^2$ (Zn) atoms, to obtain a material of "average" atoms with electron configuration $d^{10}s^1$, i.e., the electron configuration of Cu atoms. Such an argument helped to bridge the close similarity in the electronic structure of 1:1 Pd−Zn alloys and metallic Cu; slab model calculations had shown a similar surface reactivity of these two materials.[8−10]

Trends of the surface reactivity were illustrated, for instance, by the calculated adsorption energy of probe CO molecules at 3-fold-hollow sites Pd_2Zn of PdZn(111) surface, 1.0 eV (obtained with the PW91 exchange-correlation potential[35]); this value is close to that on the Cu(111) surface, ∼0.9 eV, but differs considerably from the energy of μ_3-CO adsorbed on the Pd(111) surface, ∼1.9 eV.[8] The finding that CO binds weaker to the surface of PdZn alloy than to monometallic Pd agrees with experimental observations for PdZn and Pd polycrystalline samples.[6] Thus, on Pd−Zn particles that manifest local and overall concentrations Pd/Zn higher than 1:1, it is also reasonable to expect a notable reduction of CO adsorption energies compared to those on the corresponding adsorption sites of monometallic Pd particles. In this sense, results described in the following paragraph were unexpected and deserve special remarks.

Before starting the present computational work on highly symmetric nanoparticle models, we had carried out a series of BP calculations on conventional ("planar") three-layer cluster models $Pd_{28-n}Zn_n$ (C_{3v} symmetry) with 12, 10, and 6 atoms in the first, second, and third layer, respectively. We considered adsorption of a single CO molecule at the *hcp* site of the cluster models Pd_{28}, $Pd_{27}Zn_1$(0,1), $Pd_{25}Zn_3$(3,0), $Pd_{24}Zn_4$(3,1), and $Pd_{22}Zn_8$(0,6), where the central Pd_3 unit of the upper layer was kept throughout. Quite unexpectedly, substitution of Pd by Zn resulted in an increase of the CO adsorption energy with respect to the value of 1.57 eV computed for the monometallic cluster Pd_{28}. We had studied three Pd−Zn models: (*i*) Zn substitution underneath the *hcp* site, $Pd_{27}Zn_1$(0,1), (*ii*) in the upper layer nearby the central Pd_3 moiety, $Pd_{25}Zn_3$(3,0), as well as (*iii*) in both positions, $Pd_{24}Zn_4$(3,1). The calculated CO adsorption energies were 0.06, 0.24, and 0.51 eV, larger than on the reference model CO/Pd_{28}. Only for the model $Pd_{22}Zn_6$(0,6), the adsorption energy of CO was calculated slightly, by 0.09 eV, smaller than for the reference. Our attempts to rationalize these counterintuitive results in terms of varying donation/back-donation propensity of the model systems $Pd_{28-n}Zn_n$ were unsuccessful. Finally, we attributed the adsorption energy behavior to the cluster size effects[41] which appeared to be still significant even for these moderately large metal substrate particles.[13] Actually, this latter observation was one of the important motivations for us to introduce and employ highly symmetric three-dimensional cluster models which are essentially free of size effects even for the most critical observable, namely the adsorption energy.[13−15]

The calculated characteristics of μ_3-CO adsorption complexes with three-dimensional nanocluster models $Pd_{140-n}Zn_n$ are displayed in Table 2.

The calculated bond distances exhibit only a limited variation over the series of adsorption complexes under investigation. The computed C−O distance, ∼119 pm, is very stable and varies less than 1 pm. Due to σ donation and π^* back-donation interactions with the substrate, it is elongated by 5 pm and 6 pm compared to the calculated[13] and experimental[46] values for free CO molecules, respectively. (A detailed experimental and theoretical analysis actually allows one to discriminate three-orbital interactions in the σ as well as the π channels.[47]) The Pd−C distance, 206−207 pm, is also quite stable throughout, except for the model $(CO)_8/Pd_{116}Zn_{24}$(0,24), 203 pm, which features Zn−Zn nearest-neighbor contacts that are absent in all other models inspected.

Adsorption energies were calculated for CO geometries optimized with the BP exchange-correlation potential at both the BP and the PBEN levels (see earlier section: Computational Details and Models); in passing we note that we had found the PBEN energetics for CO adsorption on Pd to be most accurate, in a quantitative agreement with experiment.[13] For the cluster $Pd_{132}Zn_8$(0,8) with eight Zn atoms located in the subsurface region, just beneath the central Pd_3 moiety on each hexagonal facet (Figure 1b), the CO adsorption energy decreased by about 10% compared to the reference $(CO)_8/Pd_{140}$. Interestingly, the CO adsorption energy remains essentially unchanged when three more Zn atoms substitute Pd atoms on every hexagonal facet, resulting in the cluster $Pd_{108}Zn_{32}$(24,8) (Figure 1d): 1.63 eV vs 1.61 eV (BP) and 1.32 eV vs 1.36 eV (PBEN). Apparently, Zn atoms in the upper layer [in the configuration (24,0)] at larger distances from the central Pd_3 unit exert only a minor effect on the CO adsorption energetics. This finding is corroborated by the equal CO binding energies on the cluster models $Pd_{116}Zn_{24}$(24,0) and Pd_{140}, 1.75 eV (BP) and 1.47 eV (BPEN); these two models differ only by Zn_{24}(24,0) atoms. Short Zn−Zn contacts, the new feature of the cluster $Pd_{116}Zn_{24}$(0,24), affect the adsorption propensity of CO molecules most noticeably, as anticipated: the binding energy values, 1.25 eV (BP) or 0.94 eV (PBEN), are 0.5 eV smaller.

One can see from Table 2 that calculated C−O vibrational frequencies on various substrate clusters $Pd_{140-n}Zn_n$ spread over a rather narrow interval 1752 ±7 cm^{-1}. Such a range of C−O frequencies considerably shifted down from the value of gas-phase CO molecules (with a calculated harmonic frequency of 2113 cm^{-1}) is typical for CO species adsorbed on transition metals and is attributed to back-donation interaction from metal *d*-orbitals to the antibonding π^* orbital of CO.[13,41] Our results reflect the local character of the C−O vibrations and of the back-donation. This vibrational mode is hardly sensitive to the more distant environment of the metal substrate; recall that the moiety Pd_3−CO is common to all models considered here, only surrounding Pd atoms are substituted by Zn. This local nature of the vibrational properties is the main reason why already small cluster models usually suffice for an accurate simulation of molecular vibrations at transition metal surfaces[48] and why this kind of observables does not exhibit a substantial cluster size dependence. At variance, the adsorption energy is a property that reflects the characteristics of metal surfaces in a global fashion.[13,15,41] This inherent difference allows one to understand why calculated CO adsorption energies and C−O stretching frequencies on $Pd_{140-n}Zn_n$ clusters do not show any correlation (Table 2).

Two types of mechanisms come to mind that influence the adsorption properties of bimetallic systems: geometric (ensemble, site, or dilution) factors and electronic effects, also known as ligand effects, which originate from alloying.[49] By keeping unchanged the Pd_3 moiety at the adsorption site in the immediate vicinity of the CO adsorbate, we suppressed structural factors and focused on electronic effects.

The adsorption-induced alteration of the electronic structure of $Pd_{140-n}Zn_n$ nanoparticles is best reflected in the stabilization of the Fermi energy ϵ_F in all the species investigated. This change is indicative of the electron density acquired by CO molecules via π^* back-donation which prevails over σ donation.[47] The stabilization is essentially the same, 0.18−0.20 eV, for all the adsorption systems except $(CO)_8/Pd_{116}Zn_{24}(0,24)$, which again deviates and furnishes a notably smaller stabilization of ϵ_F, 0.13 eV (Tables 1, 2). This reduced downward shift of ϵ_F is in line with notably weaker adsorption bonds in $(CO)_8/Pd_{116}Zn_{24}(0,24)$ than in other analogues (Table 2). Indeed, this finding can be rationalized by relating the adsorption energy of CO to the amount of electron density back-donated to its π^* orbitals from the metal substrate; all other conditions being equal (as is the case in the present situation), smaller back-donation is accompanied by weaker metal−CO interaction; in turn, a reduced amount of electron density withdrawn from the metal species implies a smaller adsorbate-induced stabilization of the Fermi energy ϵ_F.

The somewhat exceptional electronic structure properties of the system $(CO)_8/Pd_{116}Zn_{24}(0,24)$ are corroborated by the relative positions of the total Pd 4*d* band center $\Delta\epsilon_{Pd4d}$, 0.12 eV vs 0.03−0.06 eV, and the Pd 4*d* center $\Delta\epsilon_{Pd4d}(Pd_3)$ of the three Pd atoms defining the μ_3 adsorption site, 0.63 eV vs 0.37−0.43 eV (Tables 1, 2).

Conclusions

In the present work, we extended our modeling strategy based on high-level electronic structure calculations of three-dimensional metal nanoparticles to investigate bimetallic Pd−Zn species with low Zn atom concentrations varying up to ∼25%. We studied the influence of the number of Zn atoms and their location on the electronic structure and stability of $Pd_{140-n}Zn_n$ clusters with the structural arrangement derived from the bulk of fcc metals. The calculated average cluster cohesive energy decreases gradually with increasing number of Zn atoms: each Zn atom destabilizes the cluster by ∼1 eV. We also found that Zn atoms preferentially occupy positions in the surface layer of the model clusters and we identified a small transfer of electron density from Zn to Pd atoms.

For complexes with CO molecules adsorbed at 3-fold hollow Pd_3 sites of the hexagonal cluster facets, we explored how adsorption properties of bimetallic models change with respect to those of the reference cluster Pd_{140}. Calculated CO adsorption energies manifest a weakening of adsorbate−substrate interactions when Zn atoms are located in the subsurface layer of $Pd_{140-n}Zn_n$ clusters; on the other hand, Zn atoms in the surface layer seem to affect the CO adsorption energy only marginally. The absence of a correlation between calculated CO adsorption energies and vibrational C−O frequencies is assigned to the different nature of these properties: the former are *global* characteristics of adsorption systems, whereas the latter are mainly due to *local* effects.

Acknowledgment. The authors thank Dr. S. Krüger and Dr. Z. Chen for stimulating discussions. S.H. gratefully acknowledges a fellowship of the Deutsche Akademische Austauschdienst (DAAD) and support from the Postgraduate Education and Research Program in Chemistry (PERCH). This work was supported by the Deutsche Forschungsgemeinschaft via Priority Program 1091 "From Ideal to Real Systems: Bridging the Pressure and Material Gap in Heterogeneous Catalysis", and the Fonds der Chemischen Industrie (Germany).

References and Notes

(1) Ogden, J. M. *Annu. Rev. Energy Environ.* **1999**, *24*, 227.
(2) Trimm, D. L.; Önsan, Z. I. *Catal. Rev.* **2001**, *43*, 31.
(3) Iwasa, N.; Kudo, S.; Takahshi, H.; Masuda, S.; Takezawa, N. *Catal. Lett.* **1993**, *19*, 211.
(4) Takezawa, N.; Iwasa, N. *Catal. Today* **1997**, *36*, 45.
(5) Cubeiro, M. L.; Fierro, J. L. G. *J. Catal.* **1998**, *179*, 150.
(6) Rodriguez, J. A. *J. Phys. Chem.* **1994**, *98*, 5758.
(7) Rodriguez, J. A.; Kuhn, M. *J. Phys. Chem.* **1996**, *100*, 381.
(8) Chen, Z.; Neyman, K. M.; Gordienko, A. B.; Rösch, N. *Phys. Rev. B* **2003**, *68*, 075417.
(9) Chen, Z.; Neyman, K. M.; Rösch, N. *Surf. Sci.* **2004**, *548*, 291.
(10) Chen, Z.; Lim, K. H.; Neyman, K. M.; Rösch, N. To be published.
(11) Bäumer, M.; Freund, H.-J. *Prog. Surf. Sci.* **1999**, *61*, 127.
(12) Freund, H.-J. *Surf. Sci.* **2002**, *500*, 271.
(13) Yudanov, I. V.; Sahnoun, R.; Neyman, K. M.; Rösch, N. *J. Chem. Phys.* **2002**, *117*, 9887.
(14) Yudanov, I. V.; Sahnoun, R.; Neyman, K. M.; Rösch, N.; Hoffmann, J.; Schauermann, S.; Johánek, V.; Unterhalt, H.; Rupprechter, G.; Libuda, J.; Freund, H.-J. *J. Phys. Chem. B* **2003**, *107*, 255.
(15) Yudanov, I. V.; Neyman, K. M.; Rösch, N. *Phys. Chem. Chem. Phys.* **2004**, *6*, 116.
(16) Dunlap, B. I.; Rösch, N. *Adv. Quantum Chem.* **1990**, *21*, 317.
(17) Belling, T.; Grauschopf, T.; Krüger, S.; Mayer, M.; Nörtemann, F.; Staufer, M.; Zenger, C.; Rösch, N. In *High Performance Scientific and Engineering Computing*; Bungartz, H.-J., Durst, F., Zenger, C., Eds.; Lecture Notes in Computational Science and Engineering; Springer: Heidelberg, 1999; Vol. 8, p 439.
(18) Belling, T.; Grauschopf, T.; Krüger, S.; Nörtemann, F.; Staufer, M.; Mayer, M.; Nasluzov, V. A.; Birkenheuer, U.; Hu, A.; Matveev, A. V.; Shor, A. M.; Fuchs-Rohr, M. S. K.; Neyman, K. M.; Ganyushin, D. I.; Kerdcharoen, T.; Woiterski, A.; Rösch, N. ParaGauss, Version 2.2; Technische Universität München, 2001.
(19) Häberlen, O. D.; Rösch, N. *Chem. Phys. Lett.* **1992,** *199*, 491.
(20) Rösch, N.; Krüger, S.; Mayer, M.; Nasluzov, V. A. In *Recent Developments and Applications of Modern Density Functional Theory*; Seminario, J. M., Ed.; Elsevier: Amsterdam, 1996; p 497.
(21) Rösch, N.; Matveev, A.; Nasluzov, V. A.; Neyman, K. M.; Moskaleva, L.; Krüger, S. In *Relativistic Electronic Structure Theory—Applications*; Schwerdtfeger, P., Ed.; Elsevier: Amsterdam, 2004; in press.
(22) Vosko, S. H.; Wilk, L.; Nusair, M. *Can. J. Phys.* **1980**, *58*, 1200.
(23) Becke, A. D. *Phys. Rev. A* **1988**, *38*, 3098.
(24) Perdew, J. P. *Phys. Rev. B* **1986**, *33*, 8622; **1986**, *34*, 7406.

(25) Fan, L.; Ziegler, T. *J. Chem. Phys.* **1991**, *94*, 6057.
(26) Hammer, B.; Hansen, L. B.; Nørskov, J. K. *Phys. Rev. B* **1999**, *59*, 7413.
(27) Huzinaga, S. *J. Chem. Phys.* **1977**, *66*, 4245.
(28) Widmark, P.-O.; Malmqvist, P.-A.; Roos, B. O. *Theor. Chim. Acta* **1990**, *77*, 291.
(29) Nava, P.; Sierka, M.; Ahlrichs, R. *Phys. Chem. Chem. Phys.* **2003**, *5*, 3372.
(30) Boys, S. F.; Bernardi, F. *Mol. Phys.* **1970**, *19*, 553.
(31) Cubeiro, M. L.; Fierro, J. L. G. *J. Catal.* **1998**, *179*, 150.
(32) Iwasa, N.; Ogawa, N.; Masuda, S.; Takezawa, N. *Bull. Chem. Soc. Jpn.* **1998**, *71*, 1451.
(33) *CRC Handbook of Chemistry and Physics*, 77th ed.; Lide, D. R., Ed.; CRC Press: Boca Raton, 1996.
(34) Hansen, M. *Constitution of Binary Alloys*, 2nd ed.; McGraw-Hill: New York, 1958.
(35) Perdew, J. P.; Chevary, J. A.; Vosko, S. H.; Jackson, K. A.; Pederson, M. R.; Singh, D. J.; Fiolhais, C. *Phys. Rev. B* **1992**, *46*, 6671.
(36) Bradshaw, A. M.; Hoffmann, F. M. *Surf. Sci.* **1978**, *72*, 513.
(37) Guo, X.; Yates, J. T., Jr. *J. Chem. Phys.* **1989**, *90*, 6761.
(38) Loffreda, D.; Simon, D.; Sautet, P. *Surf. Sci.* **1999**, *425*, 68.
(39) Lopez, N.; Nørskov, J. K. *Surf. Sci.* **2001**, *477*, 59.
(40) *Cluster Models for Surface and Bulk Phenomena*; Pacchioni, G., Bagus, P. S., Parmigiani, F., Eds.; NATO ASI Series B, Vol. 283, Plenum: New York, 1992.
(41) Whitten, J. L.; Yang, H. *Surf. Sci. Rep.* **1996**, *24*, 59.
(42) Ferrari, A. M.; Xiao, C.; Neyman, K. M.; Pacchioni, G.; Rösch, N. *Phys. Chem. Chem. Phys.* **1999**, *1*, 4655.
(43) Boldyrev, A. I.; Simons, J. *Periodic Tables of Diatomic Molecules*; Wiley: Chichester, 1997.
(44) *Periodensystem der Elemente*; VCH: Weinheim, 1995.
(45) Chirlian, L. E.; Francl, M. M. *J. Comput. Chem.* **1987**, *8*, 894.
(46) Huber, K. P.; Herzberg, G. *Molecular Spectra and Molecular Structure. Constants of Diatomic Molecules*, Vol. IV; Reinhold: New York, 1979.
(47) Föhlisch, A.; Nyberg, M.; Bennich, P.; Triguero, L.; Hasselström, J.; Karis, O.; Pettersson, L. G. M., Nilsson, A. *J. Chem. Phys.* **2000**, *112*, 1946.
(48) Neyman, K. M.; Rösch, N.; Kostov, K. L.; Jakob, P.; Menzel, D. *J. Chem. Phys.* **1994**, *100*, 2310; (b) Neyman, K. M.; Rösch; N. *Surf. Sci.* **1994**, *307/309*, 1193; (c) Staufer, M.; Neyman, K. M.; Jakob, P.; Nasluzov, V. A.; Menzel, D.; Rösch, N. *Surf. Sci.* **1996**, *369*, 300; (d) Neyman, K. M.; Staufer, M.; Nasluzov, V. A.; Rösch, N. *J. Mol. Catal.* **1997**, *119*, 245.
(49) Nieuwenhuys, B. E. *Surf. Rev. Lett.* **1996**, *3*, 1869.